

# Temperature-driven directional coalescence of silver nanoparticles

Shi Yan,<sup>a</sup> Dongbai Sun,<sup>a</sup> Yu Gong,<sup>b</sup> Yuanyuan Tan,<sup>a</sup> Xueqing Xing,<sup>b</sup> Guang Mo,<sup>b</sup> Zhongjun Chen,<sup>b</sup> Quan Cai,<sup>b</sup> Zhihong Li,<sup>b</sup> Hongying Yu<sup>c\*</sup> and Zhonghua Wu<sup>b\*</sup>

<sup>a</sup>National Center for Materials Service Safety, University of Science and Technology, Beijing 100083, People's Republic of China, <sup>b</sup>Institute of High Energy Physics, Chinese Academy of Sciences, Beijing 100049, People's Republic of China, and <sup>c</sup>Corrosion and Protection Center, Laboratory for Corrosion-Erosion and Surface Technology, University of Science and Technology, Beijing 100083, People's Republic of China. \*Correspondence e-mail: hyu@ustb.edu.cn, wuzh@ihep.ac.cn

Received 6 September 2015

Accepted 5 February 2016

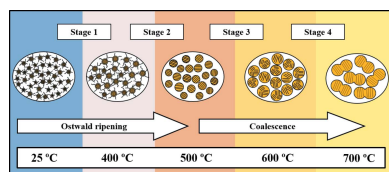
Edited by A. F. Craievich, University of São Paulo, Brazil

**Keywords:** silver nanoparticles; SAXS; XRD; coalescence; nanocrystal.

Silver nanoparticles were synthesized with a chemical reduction method in the presence of polyvinylpyrrolidone as stabilizing agent. The thermal stability behavior of the silver nanoparticles was studied in the temperature range from 25 to 700°C. Thermal gravimetric analysis was used to measure the weight loss of the silver nanoparticles. Scanning electron microscopy and high-resolution transmission electron microscopy were used to observe the morphology and the change in shape of the silver nanoparticles. *In situ* temperature-dependent small-angle X-ray scattering was used to detect the increase in particle size with temperature. *In situ* temperature-dependent X-ray diffraction was used to characterize the increase in nanocrystal size and the thermal expansion coefficient. The results demonstrate that sequential slow and fast Ostward ripening are the main methods of nanoparticle growth at lower temperatures (<500°C), whereas successive random and directional coalescences are the main methods of nanoparticle growth at higher temperatures (>500°C). A four-stage model can be used to describe the whole sintering process. The thermal expansion coefficient ( $2.8 \times 10^{-5} \text{ K}^{-1}$ ) of silver nanoparticles is about 30% larger than that of bulk silver. To our knowledge, the temperature-driven directional coalescence of silver nanocrystals is reported for the first time. Two possible mechanisms of directional coalescence have been proposed. This study is of importance not only in terms of its fundamental academic interest but also in terms of the thermal stability of silver nanoparticles.

## 1. Introduction

Metallic nanoparticles have received great attention (Burda *et al.*, 2005; Murphy *et al.*, 2008; Sudeep & Kamat, 2005) due to their unique optical, electronic, magnetic and catalytic properties, which are highly dependent on the nanoparticle size, structure and shape. Moreover, noble metal nanoparticles have often been used as model substances (Collier *et al.*, 1997; Daniel & Astruc, 2004; Sastry *et al.*, 2000) in the study of nanomaterials because they can be synthesized easily and modified chemically as well as being more suitable for application. In our previous work (Yan *et al.*, 2014), the growth behavior of silver nanoparticles in an aqueous solution of silver nitrate was carefully studied where polyvinylpyrrolidone (PVP) was used as the stabilizing agent and NaBH<sub>4</sub> as the reductant. The growth mechanism of silver nanoparticles and the nanoparticle-size dependency *versus* time were obtained. As a traditional noble metal, silver has its advantages when it comes to the nanoscale, which has attracted great interest



© 2016 International Union of Crystallography

(Ayati *et al.*, 2011; Eminian *et al.*, 2011; Fabrega *et al.*, 2011; Kaegi *et al.*, 2011) due to the unique properties and applications of silver nanoparticles. However, the thermal stability of silver nanoparticles is crucial to their application. It is well known that one nanoparticle may be amorphous or crystalline, and one crystalline nanoparticle could consist of single or multiple nanocrystals. Therefore, knowledge of the size changes of nanoparticle and nanocrystal with temperature is desired for understanding the thermal stability of nanoparticles.

Some temperature-dependent properties and applications of silver nanoparticles have been studied. Moon *et al.* (2005) investigated the low-temperature sintering behavior of silver nanoparticles synthesized with the combustion chemical-vapor condensation method. Obvious coalescence of the nanoparticles was observed while sintering the nanoparticles at 150, 200 and 250°C. It was reported that the nanoparticle and nanocrystal sizes increased with increasing annealing temperature. Volkman *et al.* (2011) studied also the sintering of silver nanoparticles at temperatures lower than 200°C. They claimed that thiol encapsulated silver nanoparticles had been annealed into conductive film. During the whole sintering process the surfactant was always existent and had great influence on the nanocrystal size and orientation of the silver nanoparticles in the resulting film. Majeed Khan *et al.* (2011) reported the crystalline structure of the silver nanoparticles synthesized with the wet chemical solution method. The lattice constant of the silver nanoparticles with face-centered cubic (f.c.c.) structure was 0.4085 nm. Further, the silver nanoparticles were re-dispersed in ethanol and a dip-coating method was used to prepare the silver nanoparticle film. It is found that the temperature dependence of the silver-film resistivity exhibited semiconducting behavior. In fact, the coalescence of nanoparticles at high-temperature is almost inevitable. However, the detailed coalescence process or mechanism between nanoparticles is scarcely mentioned in the previous studies. Usually the nanoparticle size and/or the nanocrystal size all increase with increasing temperature, but the tendencies of the nanoparticle and nanocrystal sizes to increase could be different, and were determined by the different growth methods of nanoparticles.

Coalescence is one of the main methods of nanoparticle growth. The coalescence of nanoparticles will affect the final nanoparticle morphology and performance. Therefore, knowledge of the coalescence process is crucial not only for controlling the size and morphology of nanomaterials but also for their applications. In this paper, small-angle X-ray scattering (SAXS), X-ray diffraction (XRD), scanning electron microscopy (SEM), high-resolution transmission electron microscopy (HRTEM) and thermal analysis will be used to investigate the thermal stability of silver nanoparticles. In particular, the *in situ* SAXS technique will be used to monitor the real-time change of nanoparticle size (Yan *et al.*, 2014; Kammler *et al.*, 2005; Wang *et al.*, 2008) during the heating process. We expect that this research could provide direct insight into the coalescence mechanism of silver nanoparticles.

## 2. Experiment

### 2.1. Sample preparation

The source materials AgNO<sub>3</sub>, NaBH<sub>4</sub>, BN and PVP (K-30, average MW  $\simeq$  40000) were purchased from Sinopharm Chemical Reagent Co. Ltd. All reagents were in analytical purity without further purification before use. The silver nanoparticles were synthesized with a reduction reaction method. First, AgNO<sub>3</sub> with a concentration of 25 mM and PVP with a concentration of 2.5 mM were dissolved together in distilled water as the reaction solution. Then, NaBH<sub>4</sub> with a concentration of 25 mM was also dissolved in distilled water as the reduction solution. Afterwards the fresh reduction solution (NaBH<sub>4</sub> solution) was dropped into the fresh reaction solution (AgNO<sub>3</sub> solution) at a constant rate of 30 drops per minute while stirring the reaction solution. The mixed volume ratio of the two solutions was controlled to 1:1. After the NaBH<sub>4</sub> solution ran out, stirring of the mixed solution was maintained for 30 min. Subsequently, the mixed solution was added to acetone in a volume ratio of 1:5, forming a kind of suspension. After the suspension was centrifuged at 10000 rotations per minute for 15 minutes, some precipitates were collected from the bottom of the mixed solution. The precipitate was re-dispersed into acetone and centrifuged repeatedly five times until the extra surface agent was washed away. The precipitate was dried at room temperature to obtain the silver nanoparticle powder. The whole synthesis process for silver nanoparticles was performed at room temperature (25°C).

### 2.2. Microscopic observation

To observe the morphology change of silver nanoparticles as a consequence of the sintering process, the silver nanoparticle powders placed in an alumina crucible were first annealed at 100, 200, 300, 400, 500, 600 and 700°C for more than 30 min in nitrogen atmosphere. Then, the annealed silver nanoparticle powders were dispersed in ethanol to form a suspension. Several drops of the suspension were dripped onto a clean silicon chip and Cu grid, respectively. After the ethanol evaporated, the silicon chip sample was used for SEM observation, which was performed by using a Hitachi S-4800 SEM with an accelerating voltage of 10 kV, whereas the Cu grid sample was used for HRTEM observation, which was carried out using a Jeol 2010 transmission electron microscope (TEM) with an accelerating voltage of 200 kV.

### 2.3. Thermal analysis

To analyze the weight loss of the silver nanoparticle powder during the heating process, a thermogravimetry analysis (TGA) was performed by using a TGA/DTA thermal system (TGA/DAC 1/1600 HT). In the TGA measurement, the silver nanoparticle powder was placed in a ceramic (Al<sub>2</sub>O<sub>3</sub>) crucible, which was properly protected by nitrogen atmosphere. The TGA curve of the sample was recorded at temperatures ranging from room temperature to 600°C with a heating rate of 10°C min<sup>-1</sup>. For comparison, the TGA curve of the pure

PVP sample was also measured under the same experimental conditions.

#### 2.4. SAXS measurements

For the *in situ* SAXS measurements, 50 mg of the silver nanoparticles powder and 450 mg of BN powder were mixed together and compressed into a tablet with radius of 4 mm and thickness of 1 mm. Another tablet with only 450 mg of BN powder was also prepared, which was used as the reference sample for removing the background scattering. The BN grains are at the micrometer level and about 100 times larger than the silver nanoparticles. Evidently the BN matrix has no obvious influence on the possible coalescence of silver nanoparticles located between the BN grains. Temperature-dependent SAXS measurements for the silver nanoparticles and the reference sample were performed at beamline 1W2A of Beijing Synchrotron Radiation Facility (BSRF). The incident X-ray wavelength was fixed at 1.54 Å. During the SAXS measurements the samples were heated to target temperatures with a heating rate of 10°C min<sup>-1</sup> and were then kept at each target temperature for more than 30 min before measurement. *In situ* SAXS patterns of the two samples were collected at 25, 100, 200, 300, 400, 500, 600 and 700°C for 1 s. An ion chamber in front of the sample was used to record the incident X-ray intensity. All the collected SAXS patterns were normalized to have the same incident X-ray intensity.

#### 2.5. XRD measurements

For the XRD measurements, the silver nanoparticles were first dispersed in ethanol to form a suspension. Then the suspension was dripped onto an AlN ceramic chip. After the ethanol was evaporated at room temperature, the remaining silver nanoparticles formed a slice with thickness of about 1 mm on the ceramic chip, which was used for the XRD experiment. Because the silver nanoparticle slice was sufficiently thick, the diffraction from the AlN underlayer could be completely depressed. Temperature-dependent XRD measurements for the silver nanoparticles were performed at beamline 4B9A of BSRF. The incident X-ray wavelength was fixed at 1.54 Å. During the XRD measurements, the sample was kept in a low-vacuum (0.1 Pa) heating furnace. The sample was heated to respective target temperatures with a heating rate of 10°C min<sup>-1</sup>. *In situ* XRD patterns of the sample were collected at 25, 100, 200, 300, 400, 500, 600 and 700°C for about 45 min.

### 3. Result and discussion

In order to study the coalescence behavior of silver nanoparticles, these nanoparticles have to be heated to different temperatures. In such a heating process, weight loss is often inevitable. Therefore, a thermal analysis was first performed to monitor the possible weight loss of the silver nanoparticles during the heating process. Fig. 1 compares the TGA curves between the PVP-coated silver nanoparticles and the pure PVP sample. It can be seen that both TGA curves have similar

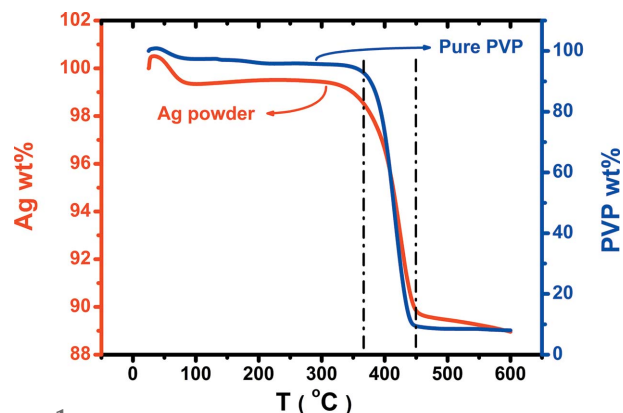


**Figure 1**  
TGA curves of the PVP-coated silver nanoparticles and the pure PVP sample.

profiles. The dominant weight loss occurred between 350 and 450°C. When the sample temperature was higher than 450°C, the weight loss of the pure PVP sample is higher than 90%. This demonstrates that the PVP has been decomposed at the higher temperatures. On the other hand, the PVP-coated silver nanoparticles have only about 15% weight loss, which can be attributed to the decomposition of PVP coated on the silver nanoparticles surface. Evidently the PVP coating on the silver nanoparticles surface was almost removed when the sample temperature was higher than 450°C.

The morphology change of the as-prepared PVP-coated silver nanoparticles with annealing temperature was recorded by the SEM images as shown in Fig. 2. Roughly, all the nanoparticles are approximately of spherical shape, and the average nanoparticle size increases slightly with the annealing temperature increasing from 25 to 500°C as shown in Figs. 2(a)–2(f). In this temperature range these silver nanoparticles are relatively stable with only a slow growth. However, an obvious increase of the nanoparticle size can be found when the annealing temperature was increased to 600°C, as shown in Fig. 2(g). The obvious larger size of the silver nanoparticles implies that a rapid growth of silver nanoparticles occurred at around 600°C. When the annealing temperature was 700°C, a dimeric even multimeric morphology of the spherical nanoparticles can be observed, as shown in Fig. 2(h). A blackberry substructure of size ~10 nm seems to form on the surface of the spherical nanoparticles. Roughly, two spherical nanoparticles were connected together to form one peanut-like silver nanoparticle. This morphological change clearly displays the coalescence behavior of the silver nanoparticles. Although the coalescence mechanism is still ambiguous, knowledge about the coalescence details is desired for controlling the morphology and size of these silver nanoparticles. Therefore, a more detailed study of the coalescence method is necessary.

HRTEM was used to observe directly the details of the coalescence interface between the nanoparticles and the interior structures within the nanoparticles. HRTEM images of the silver nanoparticles at three representative annealing temperatures are given in Fig. 3. A representative PVP-coated silver nanoparticle with annealing temperature of 300°C is

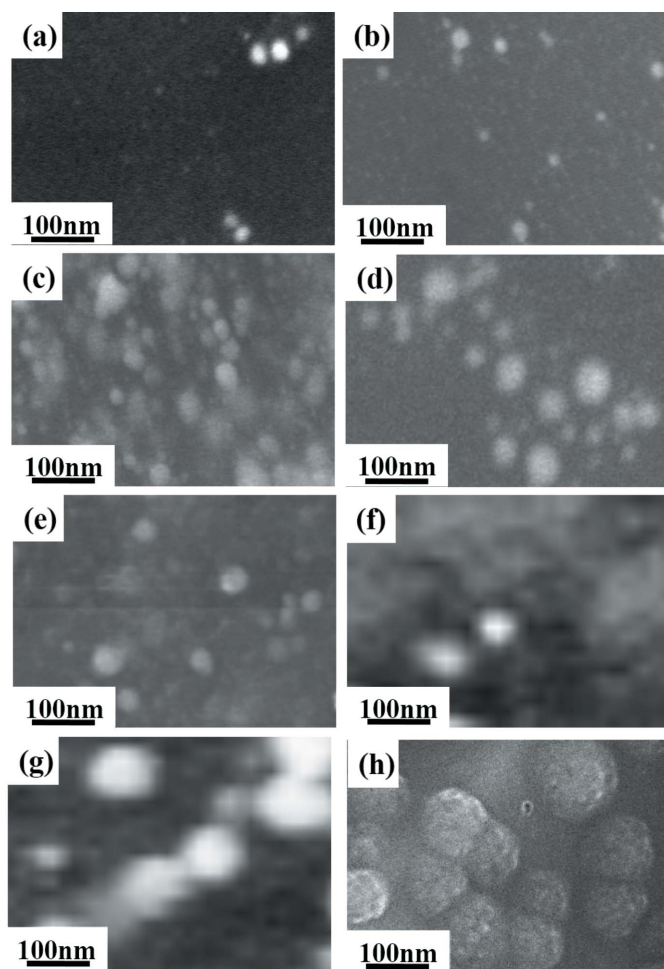


**Figure 2**  
SEM images of the PVP-coated silver nanoparticles after annealing at different temperatures. From (a) to (h), the annealing temperature is 25, 100, 200, 300, 400, 500, 600 and 700°C.

shown in Fig. 3(a). It can be seen that eye-catching fringes almost fill the whole nanoparticle, which demonstrates that the nanoparticle is in crystalline form, and one nanoparticle contains only one nanocrystal. Such a nanoparticle is about 28 nm in diameter and seems to have a thin surface layer in noncrystalline form. This noncrystalline surface layer can be ascribed to the remaining PVP residuals as confirmed by the TGA measurement. In fact, all of the silver nanoparticles have similar features in the temperature range from room temperature to 500°C except for a slower increase of nanoparticle size with annealing temperature. When the annealing temperature increased to 600°C, it was found that there are always some fringes with different orientations in each of the silver nanoparticles as shown in Fig. 3(b). The different orientations of the fringes reveal that one silver nanoparticle contains multiple silver nanocrystals after the sample was annealed at 600°C. The nanoparticle size at 600°C was confirmed to have rapidly increased by the SEM image shown in Fig. 2(g). This tells us that it was the coalescence of smaller silver nanoparticles that led to the rapid increase of the nanoparticle size. Evidently the coalescence of smaller nanoparticles is the main growth method of the silver nanoparticles

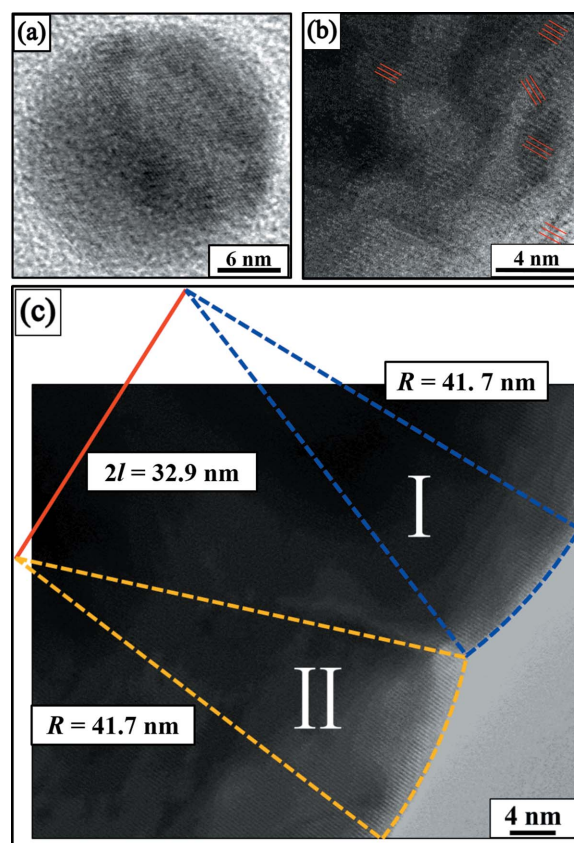


**Figure 3**  
HRTEM images of the silver nanoparticles. (a) One nanoparticle containing only one nanocrystal encapsulated in a noncrystalline surface layer after annealing at 300°C. (b) One nanoparticle containing multiple nanocrystals with different orientations after annealing at 600°C. (c) Two nanocrystals with the same orientation coalesced together to form one peanut-type nanoparticle after annealing at 700°C. The dashed lines represent the radii of the nanocrystals and the solid line connects the centers of two nanocrystals.

if they were annealed at 600°C. The nanoparticle coalescence is random without preferential coalescent orientation as confirmed by the fringes with different orientations. For the silver nanoparticles annealed at 700°C, a typical HRTEM image of the sample is shown in Fig. 3(c). Corresponding to the different morphology of the nanoparticles at 700°C from others, a completely different coalescence feature can be found from the sample annealed at 700°C. This nanoparticle can be divided into two parts (I and II) which are in tight contact together. Although the two parts have completely parallel and equal-width fringes, both can be attributed to two adjacent nanoparticles before they coalesced. That is to say, two adjacent nanoparticles were directionally coalesced when the annealing temperature was up to 700°C. From Fig. 3(c), the fringe spacing can be estimated to be about 0.2 nm, which approximates to the interplanar distance of the (200) lattice plane of silver f.c.c. structure. Therefore, it can be concluded that the [200] orientation was the coalescence direction of the crystalline silver nanoparticles when they were annealed at 700°C. Due to the directional coalescence and the complete matched coalescence planes, two coalesced silver nanocrystals

form a larger nanocrystal with peanut-type appearance. A similar coalescence morphology (dumbbell-type) was also reported (Moon *et al.*, 2005), but there is no description of the coalescence direction of the silver nanoparticles.

From the above discussion it can be determined that the nanoparticle at 600°C is polycrystalline, but the nanoparticle at 700°C is a single nanocrystal. Therefore, we believe that multiple initial nanocrystals in a nanoparticle at 600°C have been driven to have the same orientation and formed a single nanocrystal with the temperature increasing to 700°C. During the orienting ordered arrangement, these initial nanocrystals must experience rotation and movement. Although all the initial nanocrystals in a nanoparticle at 600°C have been orderly arranged and formed a single nanocrystal at 700°C, the surface of the nanoparticle must be rugged at the formation stage of the single nanocrystal because of the different initial nanocrystal sizes. This is perhaps the reason for the blackberry-like substructure on the surface of the nanoparticles at 700°C as shown in Fig. 2(h). Of course, the attachment of some smaller nanoparticles on the surface could not be excluded completely. In fact, after these initial nanocrystals in a nanoparticle formed a single nanocrystal, two adjacent nanoparticles were also directionally coalesced into a peanut-like nanoparticle as shown in Figs. 2(h) and 3(c).

To pursue quantitatively the change of the silver nanoparticle size during the heating process, *in situ* SAXS measurements were performed in the temperature range from room temperature to 700°C for the as-prepared silver nanoparticles. Because the samples were kept at each target temperature for more than 30 min, the samples were thought to be approximately in a state of equilibrium. As examples, two typical SAXS patterns of the silver nanoparticles at room temperature (25°C) and at the heating temperature of 600°C are shown in Figs. 4(a) and 4(b). It can be found that all the SAXS patterns are approximately centrosymmetric around the direct beam position without preferred orientation, which means that the silver nanoparticles are approximately randomly distributed in the sample tablet during the whole heating process. For further SAXS data analysis, all the two-

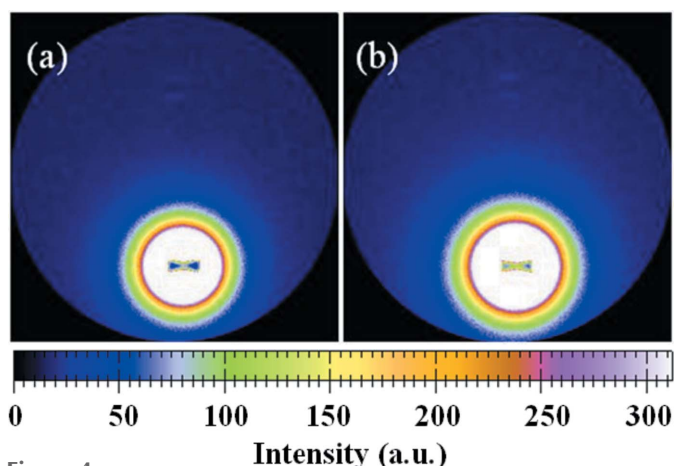


Figure 4 Two-dimensional SAXS patterns of silver nanoparticles at (a) 25°C and (b) 600°C.

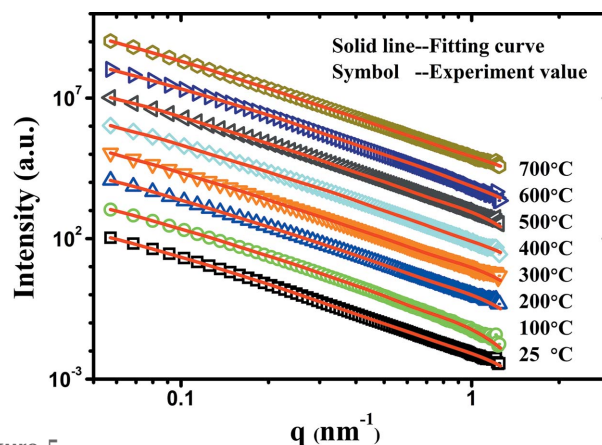
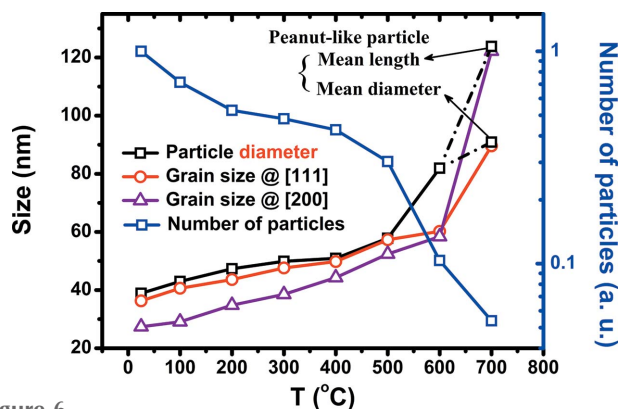


Figure 5 *In situ* SAXS intensities of silver nanoparticles at different temperatures. Solid lines are the fitting curves, and symbols represent the experimental values. To avoid overlap, these SAXS curves have been shifted along the vertical axis.

dimensional SAXS patterns were first converted to one-dimensional SAXS curves through a circular integral by using *Fit-2D* software (Hammersley, 2004). After background removal and normalizing to the incident X-ray intensity, all the SAXS curves from silver nanoparticles were extracted.

The tangent-by-tangent (TBT) method (Wang *et al.*, 2008) was used to analyze the gyration radius ( $r_g$ ) of the silver nanoparticles. The extracted SAXS intensities and the fitting curves at different temperatures are shown in Fig. 5. Although the gyration radius can be used to describe the change of nanoparticle size with heating temperature, it cannot provide information on the nanoparticle shape. Based on the SEM and HRTEM images shown in Figs. 2 and 3, these silver nanoparticles with heating temperatures lower than or equal to 600°C can be classified by a spherical shape, but the silver nanoparticles with heating temperature of 700°C can be described as peanut-like nanoparticles. From these known nanoparticle shapes and the extracted gyration radius, the real nanoparticle sizes can be calculated.

For monodisperse spherical nanoparticles, the gyration radius  $r_g = (3/5)^{1/2}d/2$ , where  $d$  is the diameter of the nanoparticle. For the polydisperse spherical nanoparticles in our case, their gyration radii have been obtained by fitting the SAXS curves with the TBT method. From these SAXS-extracted gyration radii, the average gyration radius ( $\bar{r}_g$ ) can be calculated. Therefore, the real and average diameter change of spherical nanoparticles from 25 to 600°C can be calculated by  $d = 2(5/3)^{1/2}\bar{r}_g$  as shown in Fig. 6. Due to a certain shape-deviation of the silver nanoparticle from spherical and their size polydispersity, the error bars of the estimated average diameters are about  $\pm 3$  nm. The SAXS results demonstrate that the diameter of the spherical silver nanoparticles increases linearly from 38.9 to 57.8 nm with the heating temperature increasing from 25 to 500°C; the growth rate is about 4.2 nm per 100°C. Then the nanoparticle diameter increases from 57.8 to 81.9 nm with the heating temperature increasing from 500 to 600°C; the growth rate is about 24.1 nm per 100°C. These SAXS results also confirm


**Figure 6**

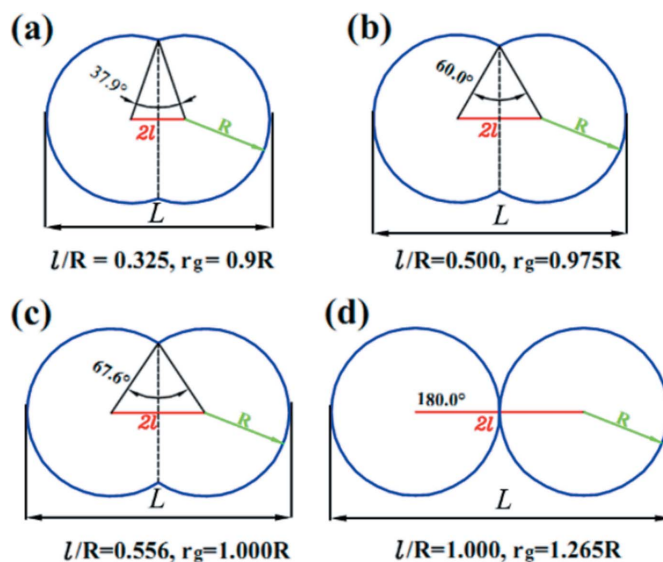
Change of silver-nanoparticle diameter and number, as well as nanocrystal sizes, with heating temperature. From 600 to 700°C the spherical silver nanoparticle becomes a peanut-like one where two parameters (mean length and mean diameter) are used to describe its size as shown by the dot-dashed lines.

that the silver nanoparticle size experiences a slower increase from 25 to 500°C, then a rapid increase from 500 to 600°C. The lower-temperature (<500°C) growth can be ascribed to an Ostwald ripening (Challa *et al.*, 2011) progress, while the higher-temperature (500–600°C) growth can be ascribed to a coalescence process. In this coalescence region, two or even more silver nanoparticles were randomly coalesced together to form a larger silver nanosphere.

For peanut-type nanoparticles, as in the sample with heating temperature of 700°C, their gyration radius  $r_g$  depends on the distance between two spherical nanoparticles and the radii of the two spherical nanoparticles in a peanut-like nanoparticle. Assuming that the two spherical nanoparticles have the same radius ( $R$ ) and the distance between the two centers of spherical nanoparticles is  $2l$ , where  $0 < l < R$ , then the gyration radius  $r_g$  of the peanut-type nanoparticle can be deduced and expressed as follows:

$$r_g(R, l) = \left( \frac{12R^5 + 30R^4l + 20R^3l^2 + 2l^5}{20R^3 + 30R^2l - 10l^3} \right)^{1/2}. \quad (1)$$

In fact, if the coalescence contour of two spherical nanoparticles into one peanut-like nanoparticle is known, then the distance  $2l$  between the centers of two spherical nanoparticles and the radius  $R$  of two spherical nanoparticles can be easily calculated on the basis of the gyration radius  $r_g$  extracted from SAXS. Four coalescence contours of the peanut-like nanoparticles are schematically shown in Fig. 7. Evidently, the larger the  $l/R$  ratio or the lower the coalescence degree, then the larger the gyration radius of the peanut nanoparticle. From the contour or the intersection angle  $2\theta$  of the peanut-like nanoparticle, the  $l/R$  ratio can be obtained. Combining with the obtained gyration radius  $r_g$ , then the real radius  $R$  of spherical nanoparticles and the largest dimension  $2(R + l)$  of the peanut-like nanoparticle can be obtained on the basis of equation (1). For example, if  $l/R = 0.556$ , then  $r_g = R$ . The largest dimension  $L$  of the peanut-like nanoparticle will be  $3.112r_g$ .


**Figure 7**

Coalescence of two spherical nanoparticles with radius  $R$  into one peanut-like nanoparticle. The distance between the two centers of spherical nanoparticles is  $2l$ . Four typical coalescence shapes of the peanut nanoparticles with different sphere-center distance  $2l$  or intersection angle  $2\theta$  and gyration radius  $r_g$  are shown.

From the SAXS analysis, the average gyration radius of silver nanoparticles at 700°C was obtained to be about 41.7 nm, while the  $l/R$  ratio can be estimated to be about 0.364 from Fig. 3(c) for the peanut-like silver nanoparticles. Thus, the diameter of the spherical part  $2R \simeq 2.18r_g = 90.9$  nm. The length of the peanut nanoparticle  $L \simeq 2.97r_g = 123.8$  nm. The center distance  $2l \simeq 32.9$  nm between the two spherical parts. These SAXS-extracted  $2l$  and  $R$  values of the peanut-like nanoparticle are also given in Fig. 3(c). The shape parameter  $l/R$  of a peanut-like nanoparticle can be easily estimated from a complete image of the nanoparticle, *i.e.*  $l/R = (L - 2R)/(2R)$ . In principle, the peanut-like nanoparticles could have different  $l/R$  ratios. If considering only the case where two identical spherical nanoparticles are coalesced into one peanut-like nanoparticle, the lengths of the peanut-like nanoparticles are possibly distributed in the range from  $R$  to  $2R$  as implied by Fig. 7. In fact, these silver nanoparticles are a polydisperse system. When two spherical nanoparticles with different radii ( $R_1, R_2$ ) are coalesced together in a similar coalescence scheme as shown in Fig. 7, the gyration radius can be expressed as a more complicated function of  $R_1, R_2$  and  $2l$ , where  $2l$  has the same definition as in equation (1). When  $R_1 \simeq R_2$ , which is our case as shown in Fig. 2(h), equation (1) is a very good approximation of its gyration radius. If  $R_1 \ll R_2$ ,  $r_g = (3/5)^{1/2}R_2$  is an appropriate approximation. For the other case, the gyration radius of a coalesced particle consists of two semispherical parts ( $R_1, R_2$ ) located between  $r_g(R_1, 2l)$  and  $r_g(R_2, 2l)$ . If more than two isometrical nanospheres are coalesced together one by one, the length of the peanut-like nanoparticles could obviously be larger, and the gyration radius extracted from SAXS data could also be larger than the average diameter of the nanospheres. However, this is not true for our case as judged from the SAXS results, although the

SEM image shown in Fig. 2(h) seems to have such a false appearance. Therefore, the silver nanoparticles with annealing temperature of 700°C can be considered approximately as a homogeneous system, in which the peanut-like nanoparticles consist of two nanoparticles. The average length and diameter of the peanut-like silver nanoparticles at 700°C are also shown in Fig. 6. In comparison with the nanoparticle size at 600°C, the nanoparticle diameter increases from 81.9 to 90.9 nm, but the nanoparticle length increases from 81.9 to 123.8 nm at 700°C. This result demonstrates that the silver nanoparticles tend to have a preferential growth direction when the annealing temperature reaches up to 700°C. Combining with the HRTEM observation, this preferential growth can be attributed to the temperature-driving directional coalescence of the silver nanoparticles.

Besides the nanoparticle size, the change of nanoparticle number is also an important parameter for the analysis of the nanoparticles' stability. Generally, the SAXS intensity at  $q = 0$  of a polydisperse nanoparticle system can be written as  $I(q = 0) = N\langle V^2 \rangle (\Delta\rho)^2$  (Polte *et al.*, 2010), where,  $\langle V^2 \rangle$  is the average of the volume square of these nanoparticles and  $N$  is the isovolumic nanoparticle number if assuming that all particles take the same volume  $V$ .  $\Delta\rho$  is the electron density contrast between the nanoparticles and the matrix. The SAXS intensity  $I(q = 0)$  can be obtained by extrapolating the SAXS curve to  $q = 0$  with the Guinier formula. Consequently, the relative nanoparticle number can be obtained by comparing the SAXS intensities  $I(q = 0)$ . The change of nanoparticle number with heating temperature is also shown in Fig. 6. It should be noted that the isovolumic particle number is not exactly the real particle number; however, the isovolumic particle number has a similar temperature-dependency with the real particle number for a unimodal polydisperse system, and can be used to assess the change of the real particle number with temperature. This result verifies that the nanoparticle number is descending with increasing heating temperature. In particular, the slower decrease of nanoparticle number at lower temperatures (<500°C) corresponds to the Ostwald ripening (Challa *et al.*, 2011) process, while the fast decrease of nanoparticle number at higher temperatures (>500°C) corresponds to the coalescence growth process.

It is well known that the SAXS technique is sensitive to the nanoparticle information, but the XRD technique is sensitive to the nanocrystal information. Generally, the SAXS/WAXS technique is used to collect the SAXS and WAXS patterns simultaneously. However, the SAXS and the WAXS measurements were performed separately in this study because of the different experimental requirements. In the SAXS measurements the powdered silver nanoparticles were mixed with the diluent BN to reach an optimal thickness for transmission SAXS. Evidently, such a SAXS sample is not suitable for collecting its XRD patterns. First, the transmission mode cannot acquire a large enough ( $2\theta \geq 90^\circ$ ) diffraction angle for the inorganic silver nanoparticles with small  $d$ -spacing at the angstrom level. Second, the unwanted diffraction peaks from the diluent BN will disturb the diffraction pattern of silver nanoparticles. Third, the angular resolution of

WAXS is lower than that of normal XRD with diffractometer. Therefore, the same silver nanoparticles were prepared in an ethanol suspension, and then were dripped on ceramic substrate to form a slice with thickness of about 1 mm after ethanol evaporation. Bragg reflection mode was used to collect the XRD patterns up to  $90^\circ$ . For the comparability between the particle size from SAXS and the nanocrystal size from XRD, the silver nanoparticles were heated to the same target temperatures and were heat-preserved for a sufficiently long time. The mutual supporting results from SAXS and XRD measurements confirm further the comparability of SAXS and XRD results.

To extract the change of nanocrystals in the heating process of the silver nanoparticles, temperature-dependent XRD measurements were performed. These collected XRD patterns were approximately in a state of equilibrium because the sample was maintained at each target temperature for more than 45 min. The *in situ* XRD patterns of the silver nanoparticles are shown in Fig. 8. It can be seen that all these diffraction peaks can be indexed to a f.c.c. structure without any detectable diffraction peaks from phase change, impurity or the ceramic substrate. From 25 to 600°C, the profiles of the diffraction patterns are almost the same, which implies that the shape of the silver nanocrystals has no obvious change in this temperature region. However, the relative intensity of the (200) reflection shows a sharp increase for the sample with heating temperature of 700°C. It is well known that only these ( $hkl$ ) planes parallel to the sample surface contribute to the ( $hkl$ ) reflection in a symmetrical Bragg–Brentano diffraction geometry. The increase of the relative intensity of the (200) reflection means that silver nanocrystals tend to a preferential orientation along the [200] orientation around 700°C. Combining the HRTEM image shown in Fig. 3(c), the peanut-like particle shape in Fig. 2(h) and the above SAXS results, it can be concluded that the silver nanocrystals were directionally coalesced together through the (200) crystal plane instead of through the (111) crystal plane.

The silver nanocrystal size ( $D$ ) can also be evaluated from the XRD pattern by using Scherrer's formula (Klug & Alexander, 1954):  $D = 0.94\lambda/\beta\cos\theta$ , where  $\lambda$  is the incident X-ray

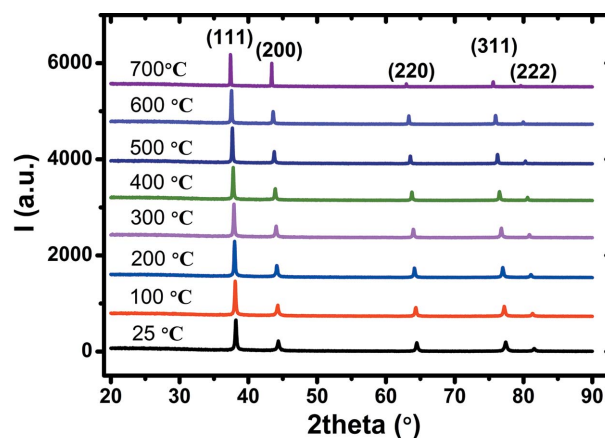


Figure 8 *In situ* XRD patterns of silver nanoparticles collected at beamline 4B9A of BSRF with an incident X-ray wavelength of 1.54 Å.

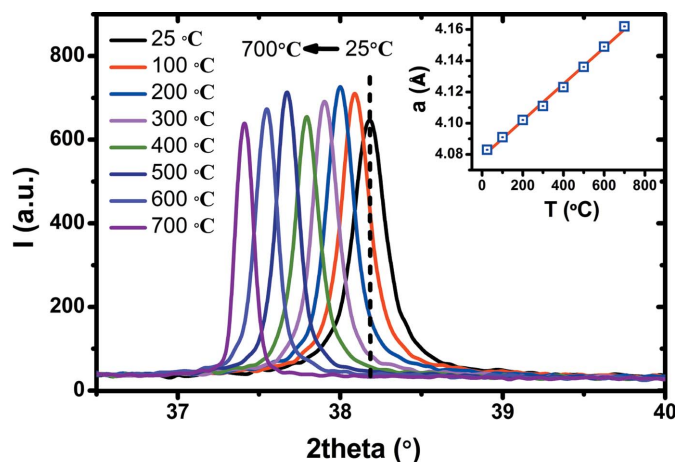


Figure 9

Position shift of the (111) reflection of the silver nanoparticles with increasing temperature. The dashed line indicates the peak position of a reference at room temperature. The corresponding lattice constants (open squares) are shown in the inset, which can be linearly fitted (solid line) to obtain the linear coefficient ( $2.8 \times 10^{-5} \text{ K}^{-1}$ ) of thermal expansion.

wavelength ( $1.54 \text{ \AA}$ ),  $\beta$  is the full width at half-maximum (FWHM) in radians of the diffraction peak, and  $\theta$  is Bragg's diffraction angle. The amplified (111) reflections are compared in Fig. 9. Obviously, the peak width is decreasing with the increase of the heating temperature, implying an increase of the nanocrystal size with heating temperature. The (111) and (200) reflections were used to evaluate the nanocrystal sizes along the [111] and [200] orientations. The estimated nanocrystal sizes are also shown in Fig. 6. It can be seen that the nanocrystal size along the [111] orientation is larger than that along the [200] orientation when the heating temperature is lower than or equal to  $500^\circ\text{C}$ , but the sizes of the nanocrystals along these two directions tend to be the same for temperature increasing up to  $600^\circ\text{C}$ . This result illustrates that the as-prepared silver nanocrystals are not ideal spheres. Previous works (Sun *et al.*, 2003; Gao *et al.*, 2005) verify that PVP molecules have a stronger interaction with the (200) than the (111) facets in the silver nanocrystals. Therefore, this stronger interaction between PVP molecules and (200) facets is more tendentious to depress the growth of the [200] orientation. Therefore, the [111] orientation was the growth direction of the PVP-coated silver nanoparticles at room temperature. When the PVP decomposition is almost complete, as at  $600^\circ\text{C}$ , the growth of silver nanocrystals is faster along the [200] orientation than along the [111] orientation, which implies that the nanocrystal size along the [200] orientation increases up to almost the same size as that along the [111] orientation. Therefore, the silver nanocrystals tend to a more spherical symmetry with the heating temperature increasing from 25 to  $600^\circ\text{C}$ . When the heating temperature was further increased to  $700^\circ\text{C}$ , the [200] orientation had a faster growth rate than the [111] orientation, and the nanocrystal size along the [200] orientation was markedly larger than that along the [111] orientation at  $700^\circ\text{C}$ . This result confirms again that the silver nanocrystals were directionally coalesced together along the [200] orientation. Evidently, the [111] orientation is the easy-

growing direction if PVP molecules are attached on the surface of the silver nanocrystals; otherwise the [200] orientation is the easy-growing direction for the naked silver nanocrystals.

By comparing the results of SAXS and XRD measurements, it can be found that the nanoparticle size is a little larger than the nanocrystal size along the [111] orientation (less than 3 nm) from room temperature to  $400^\circ\text{C}$ . This size difference can be attributed to a thin amorphous layer (1–2 nm) coating on the silver nanocrystal surface as shown in Fig. 3(a). Such an amorphous layer could be the residual PVP molecules. In addition, the deviation of particle shape from spherical and the polydisperse silver nanoparticle sizes could also give rise to an overestimation (Glatter & Kratky, 1982) of the particle sizes. When the heating temperature rises from 400 to  $500^\circ\text{C}$ , most of the PVP molecules coated on the surface of the silver nanocrystals decomposed. Due to the relatively weaker interaction between PVP molecules and the (111) facets as compared with the (200) facets, the (111) facets were essentially uncovered by PVP at 400 and  $500^\circ\text{C}$ , thus the nanocrystals grew up along the [111] orientation to have nearly the same size as the nanoparticles. The analogous nanoparticle size and nanocrystal size confirms that one silver nanoparticle contains on average one silver nanocrystal. For samples with temperature lower than  $600^\circ\text{C}$ , it can be found from Fig. 6 that the nanocrystal size along the [111] direction is about 20% larger than that along the [200] direction. In addition, the included angle between the [111] and [200] directions in a f.c.c. structure is about  $54.7^\circ$ . If considering the [111] direction as the long axis of such a nanocrystal, then the  $[2\bar{1}\bar{1}]$  direction is its short axis. In this case the long axis is approximately 28% larger than the short axis. This shape deviation from an ideal sphere has been confirmed by the SEM images as shown in Figs. 2(a)–2(f). However, there are also some quasi-spherical nanoparticles or nanocrystals in the samples as confirmed by the TEM image shown in Fig. 3(a). Generally speaking, the nanoparticle shape is not ideal but approximating to a sphere in the temperature range from 25 to  $500^\circ\text{C}$ . When the heating temperature increases from 500 to  $600^\circ\text{C}$ , the nanoparticle size increases to 81.9 nm, while the nanocrystal size is only 58.4 nm in the [200] orientation or 60.2 nm in the [111] orientation. The mean nanoparticle volume is about 2.5 times larger than the mean nanocrystal volume at  $600^\circ\text{C}$ . It can be deduced that there are about 2–3 nanocrystals to be aggregated into one nanoparticle. Combining the HRTEM observation (Fig. 3b) and the XRD pattern (Fig. 8), it can be concluded that the silver nanoparticles experienced mainly a random aggregation process of silver nanocrystals in the temperature region  $500$ – $600^\circ\text{C}$ . When the annealing temperature increases further from 600 to  $700^\circ\text{C}$ , the nanocrystal size along the [111] orientation increases to 89.6 nm and is very close to the nanoparticle diameter (90.9 nm) of the spherical parts in the peanut-type nanoparticles. Simultaneously, the nanocrystal size along the [200] orientation grows abruptly to 122.2 nm, which is about twice as large as that (58.4 nm) at  $600^\circ\text{C}$  and almost the same average length (123.8 nm) of the peanut-like nanoparticles

derived from SAXS experiments. The analogous length and diameter between the nanoparticle and the nanocrystal demonstrate that one nanoparticle contains only one nanocrystal at 700°C. It is also noteworthy that the fast increase of nanoparticle size is accompanied by a fast decrease of nanoparticle number as the heating temperature increases from 500 to 700°C. All these results confirm again that the silver nanoparticles were directionally coalesced together and the [200] orientation is the coalescence direction. Combining the HRTEM observation (Fig. 3c) and the XRD pattern (Fig. 8), it can be concluded that temperature-driven directional coalescence of silver nanocrystals is the main method of silver nanoparticle growth in the temperature region 600–700°C.

The thermal expansion behavior of these silver nanoparticles can also be analyzed from their XRD patterns. Fig. 9 compares the position change of the (111) reflections. A reference (ICSD code 44387) peak position of the silver (111) reflection is also marked by the dashed line, which corresponds to a lattice constant of 0.4086 nm as shown in Fig. 9. It can be found that the (111) peak position shifts toward lower angle, indicating a lattice thermal expansion with increasing temperature. Based on the peak positions of the (111) reflections, the lattice constants of the silver nanocrystals are estimated as shown in the inset of Fig. 9. The lattice constant of the silver nanocrystals at room temperature was obtained to be 0.4081 nm, which is almost the same as the reference. The change of lattice constant with temperature is approximately linear. The linear coefficient of thermal expansion was evaluated to be about  $2.8 \times 10^{-5} \text{ K}^{-1}$ , which is about 30% larger than that (Brandes & Brook, 1983) of bulk silver ( $2.2 \times 10^{-5} \text{ K}^{-1}$ ). Hu *et al.* (2005) studied the thermal expansion behaviors of silver nanoparticles dispersed within mesoporous silica using the *in situ* XRD technique. The obtained thermal expansion coefficients in ambient air ( $1.7 \times 10^{-5} \text{ K}^{-1}$ ) and vacuum ( $0.6 \times 10^{-5} \text{ K}^{-1}$ ) were all found to be smaller than that of bulk silver. Dubiel *et al.* (2001) also studied the thermal expansion behaviors of silver nanoparticles embedded in a silicate glass matrix by using the extended X-ray absorption fine-structure technique. It was found that the thermal expansion coefficient of 3.2 nm nanoparticles increased by about 70% whereas 5.1 nm nanoparticles showed no changes as compared with that ( $\sim 1.5 \times 10^{-5} \text{ K}^{-1}$ ) of silver foil. Jiang *et al.* (2001) calculated the relationship between lattice contraction and nanoparticle size for free surface nanoparticles. For silver nanoparticles, the calculated result shows that nanoparticles with a diameter larger than 10 nm have little effect on lattice contraction. It is well known that the unique performances of nanomaterials can be attributed to the decrease of particle volume and the increase of particle specific surface. Generally, the more the nanocrystal size decreases, the larger the nanocrystal performance deviates from its bulk counterpart; and the hydrostatic pressure on the nanocrystal surface induced by intrinsic surface stress will result in lattice contraction or lattice strain. In our case, the average nanocrystal sizes are about 36.3 nm in the [111] orientation or 27.4 nm in the [200] orientation at room temperature. The lattice parameter of the silver nanocrystals

is about 0.4081 nm, which indeed has a small contraction compared with that (0.4086 nm) of the bulk silver. However, the thermal expansion coefficient of silver nanocrystals is about 30% larger than that of bulk silver, which means that the silver nanocrystal lattice has a faster expansion with increasing temperature compared with bulk silver. In other words, the intrinsic surface stress of the silver nanocrystal or the hydrostatic pressure on the nanocrystal surface decreases in a faster way with increasing temperature compared with bulk silver. Thus, the larger thermal expansion coefficient of silver nanocrystals compared with bulk silver could be mainly attributed to a faster decrease of surface/interface energy with the increase of heating temperature.

Although the silver nanocrystals could be coalesced together at heating temperatures higher than 500°C, the coalescence behavior of silver nanocrystals is different. The above discussion demonstrates that several silver nanocrystals are coalesced together with different crystallographic orientation, meaning that the silver nanoparticles are obviously larger than the nanocrystals at 600°C. But the grown nanocrystal has almost the same size as the peanut-like nanoparticle at 700°C because on average two grown silver nanocrystals came, respectively, from two adjacent nanoparticles coalesced together along the [200] orientation. This result demonstrates that the silver nanocrystals coalesced in a silver nanoparticle tend to take the same orientation with an increase of heating temperature. On the one hand, these small nanocrystals in a nanoparticle are driven to have the same crystallographic orientation and form a single nanocrystal with temperature increasing from 600 to 700°C. On the other hand, two adjacent nanocrystals are directionally coalesced together to form a large peanut-like nanocrystal at 700°C. Evidently there is an orientation-unified process of the silver nanocrystals with an increase of heating temperature. For a cubic crystal, a theoretical calculation (Nicholas, 1968) demonstrated that the surface energy ( $\gamma$ ) of different lattice planes is different and  $\gamma(200) > \gamma(220) > \gamma(111)$ . To compensate for the increase of volume free energy caused by the temperature increasing, the silver nanocrystals must decrease the surface energy through depressing the appearance of the (200) plane. Consequently, the [200] orientation becomes an easy-growing direction. How to proceed with such an orientation-unified change in the silver nanoparticles is not yet completely clear. Here, two possible methods are proposed. (i) The boundary migration mechanism. In this mechanism it is assumed that the migration of silver atoms occurs between adjacent silver nanocrystals. The silver atoms from the smaller nanocrystals are gradually migrated onto the (200) plane of the larger nanocrystals, behaving as the boundary migration of the silver nanocrystals. In the final stage, the smaller nanocrystal is completely migrated to the larger nanocrystal to form a growing nanocrystal. This mechanism could be dominant with annealing temperatures below 500°C. (ii) The interface slide mechanism. In this mechanism it is assumed that there is a wedge-shaped interface region between two (200) facets that belong to two respective adjacent silver nanocrystals. The silver atoms in the interface region are more disordered. Thermal agitation

causes interface sliding or interface region reconstruction by moving the interface atoms from the thick end to the thin end of the interface region. As a consequence, the nanocrystals have a relative rotation and movement. Simultaneously the interface is more ordered. Finally, the two adjacent nanocrystals have the same orientation and are directly coalesced together to form a nanocrystal. This mechanism could be dominant with the heating temperature in the range 600–700°C.

In summary, the whole sintering process of PVP-coated silver nanoparticles can be roughly classified into four stages. The first stage is in the temperature range from 25 to 400°C. Here, the silver nanoparticles are coated by PVP molecules. One nanoparticle contains one nanocrystal. The [111] orientation is the easy-growing direction of the silver nanocrystals. Ostwald ripening (Challa *et al.*, 2011) is the main method of nanoparticle growth. Although the average particle diameter is near to or larger than 40 nm in this stage, we still cannot deny that there are always some Ag nanoparticles smaller than the critical size in these samples with temperature even increasing to 600°C. Some smaller particles can even be directly observed from the SEM images as shown in Figs. 2(a)–2(g). There are also some much smaller and invisible Ag nanoparticles in the samples. It should be noted that the tiny particles with size smaller than 1 nm are often difficult to detect by the SEM, SAXS and XRD techniques. We also notice that the critical size of Ni nanoparticles was claimed to be 6 nm by Challa *et al.* (2011). Therefore, Ostwald ripening was supposed to be the main method of particle growth in this stage. In addition, the atoms are transported from nanoparticles smaller than the critical size to nanoparticles larger than the critical size, which makes the smaller nanoparticles disappear and the larger ones increase in size. This Ostwald ripening (Challa *et al.*, 2011) is quite slow because the coated PVP on the surface of the silver nanoparticles forms a barrier to the growth of the nanoparticles.

The second stage is in the temperature range from 400 to 500°C. In this stage most PVP molecules coated on silver nanoparticles have been decomposed. The barrier to depress the growth of the [200] direction is removed, and thus the [200] orientation becomes the easy-growing direction of the silver nanocrystals. One nanoparticle contains one nanocrystal, but the nanoparticles have a more spherical symmetry. Ostwald ripening (Challa *et al.*, 2011) is still the main method of the nanoparticle growth.

The third stage is in the temperature range from 500 to 600°C. In this stage, on average, several smaller initial nanocrystals are randomly aggregated into one nanoparticle, resulting in a faster increase of nanoparticle size. Random coalescence is the main method of nanoparticle growth.

The fourth stage is in the temperature range from 600 to 700°C. In this stage one nanoparticle contains only one

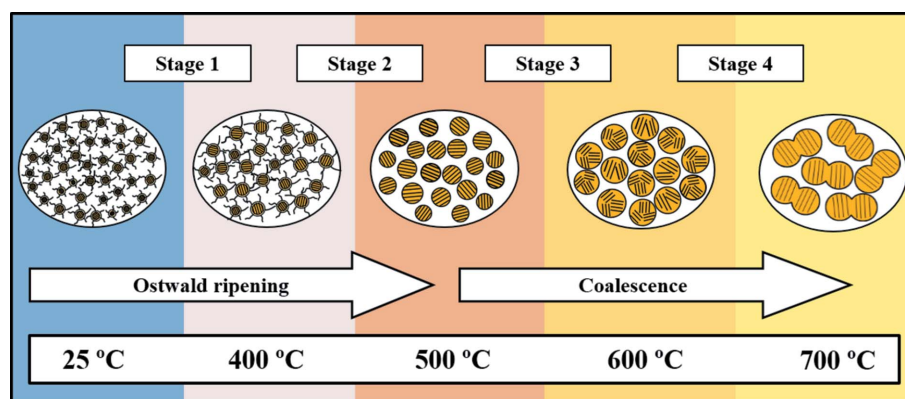


**Figure 10**  
Sketch of the growth process of PVP-coated silver nanoparticles.

nanocrystal, but the nanoparticles have a peanut-like shape. Directional coalescence is the dominant method of nanoparticle growth, leading to a fast growth of nanoparticle and nanocrystal sizes. The [200] orientation is the coalescence direction. During the coalescence growths from 500 to 700°C, the orientation-unified process of silver nanocrystals is gradually developed. A sketch map to describe the sintering process of the PVP-coated silver nanoparticles is given in Fig. 10.

#### 4. Conclusion

The thermal stability of PVP-coated silver nanoparticles was investigated by using TGA, SEM, HRTEM, *in situ* SAXS and *in situ* XRD techniques. Most of the PVP molecules coated on the silver nanoparticles are decomposed at around 400°C. The thermal expansion coefficient ( $2.8 \times 10^{-5} \text{ K}^{-1}$ ) of the silver nanoparticles is about 30% larger than that of bulk silver. A four-stage model can be used to describe the changing process of nanoparticle morphology and size from 25 to 700°C. The first stage from 25 to 400°C behaves as a slower Ostwald ripening process. Silver nanoparticles are coated with PVP and the [111] orientation is the easy-growing direction. The second stage from 400 to 500°C behaves as a faster Ostwald ripening process. Silver nanoparticles are not coated with PVP and the [200] orientation is the easy-growing direction. The third stage from 500 to 600°C behaves as a random coalescence process. Several silver nanocrystals are coalesced into a quasi-spherical silver nanoparticle. The fourth stage from 600 to 700°C behaves as a directional coalescence process. On average two nanocrystals are directionally coalesced into a nanocrystal along the [200] crystallographic orientation to form a peanut-like nanoparticle. The [200] orientations of silver nanocrystals are gradually unified by rotation and movement in the temperature range from 500 to 700°C due to the temperature-driving. Two possible mechanisms of the directional coalescence have been proposed.

#### Acknowledgements

This work was supported by the National Natural Science Foundation (No. U1232203, U1432104, 11405199, 51374019,

11305198, U1332107, 11291085) and the National Key Basic Research Program (No. 2014CB643302) of China.

References

Ayati, A., Ahmadpour, A. & Rashidi, H. (2011). *J. Nanostruct. Chem.* **2**, 15–22.

Brandes, E. A. & Brook, G. B. (1983). *Smithells Metals Reference Book*, 6th ed. London: Butterworth-Heinemann.

Burda, C., Chen, X., Narayanan, R. & El-Sayed, M. A. (2005). *Chem. Rev.* **105**, 1025–1102.

Challa, S. R., Delariva, A. T., Hansen, T. W., Helveg, S., Sehested, J., Hansen, P. L., Garzon, F. & Datye, A. K. (2011). *J. Am. Chem. Soc.* **133**, 20672–20675.

Collier, C. P., Saykally, R. J., Shiang, J. J., Henrichs, S. E. & Heath, J. R. (1997). *Science*, **277**, 1978–1981.

Daniel, M. C. & Astruc, D. (2004). *Chem. Rev.* **104**, 293–346.

Dubiel, M., Brunsch, S. & Tröger, L. (2001). *J. Synchrotron Rad.* **8**, 539–541.

Eminian, C., Haug, F. J., Cubero, O., Niquille, X. & Ballif, C. (2011). *Prog. Photovolt. Res. Appl.* **19**, 260–265.

Fabrega, J., Luoma, S. N., Tyler, C. R., Galloway, T. S. & Lead, J. R. (2011). *Environ. Intl.* **37**, 517–531.

Gao, Y., Jiang, P., Song, L., Liu, L., Yan, X., Zhou, Z., Liu, D., Wang, J., Yuan, H., Zhang, Z., Zhao, X., Dou, X., Zhou, W., Wang, G. & Xie, S. (2005). *J. Phys. D*, **38**, 1061–1067.

Glatter, O. & Kratky, O. (1982). *Small Angle X-ray Scattering*. London: Academic Press.

Hammersley, A. (2004). *FIT2D*, <http://www.esrf.eu/computing/scientific/FIT2D> (accessed November 2012).

Hu, J., Cai, W., Li, C., Gan, Y. & Chen, L. (2005). *Appl. Phys. Lett.* **86**, 151915.

Jiang, Q., Liang, L. H. & Zhao, D. S. (2001). *J. Phys. Chem. B*, **105**, 6275–6277.

Kaegi, R., Voegelin, A., Sinnet, B., Zuleeg, S., Hagendorfer, H., Burkhardt, M. & Siegrist, H. (2011). *Environ. Sci. Technol.* **45**, 3902–3908.

Kammler, H. K., Beaucage, G., Kohls, D. J., Agashe, N. & Ilavsky, J. (2005). *J. Appl. Phys.* **97**, 054309.

Klug, H. P. & Alexander, L. E. (1954). *X-ray Diffraction Procedures for Polycrystalline and Amorphous Materials*. New York: Wiley.

Majeed Khan, M. A., Kumar, S., Ahamed, M., Alrokayan, S. A. & Alsalhi, M. S. (2011). *Nanoscale Res. Lett.* **6**, 434.

Moon, K.-S., Dong, H., Maric, R., Pothukuchi, S., Hunt, A., Li, Y. & Wong, C. (2005). *J. Elec Mater.* **34**, 168–175.

Murphy, C. J., Gole, A. M., Stone, J. W., Sisco, P. N., Alkilany, A. M., Goldsmith, E. C. & Baxter, S. C. (2008). *Acc. Chem. Res.* **41**, 1721–1730.

Nicholas, J. F. (1968). *Aust. J. Phys.* **21**, 21–34.

Polte, J., Erler, R., Thünemann, A. F., Sokolov, S., Ahner, T. T., Rademann, K., Emmerling, F. & Kraehnert, R. (2010). *ACS Nano*, **4**, 1076–1082.

Sastry, M., Gole, A. & Sainkar, S. R. (2000). *Langmuir*, **16**, 3553–3556.

Sudeep, P. K. & Kamat, P. V. (2005). *Chem. Mater.* **17**, 5404–5410.

Sun, Y., Mayers, B., Herricks, T. & Xia, Y. (2003). *Nano Lett.* **3**, 955–960.

Volkman, S. K., Yin, S., Bakhishev, T., Puntambekar, K., Subramanian, V. & Toney, M. F. (2011). *Chem. Mater.* **23**, 4634–4640.

Wang, W., Chen, X., Cai, Q., Mo, G., Jiang, L. S., Zhang, K., Chen, Z. J., Wu, Z. H. & Pan, W. (2008). *Eur. Phys. J. B*, **65**, 57–64.

Yan, S., Wu, Z. H., Yu, H. Y., Gong, Y., Tan, Y. Y., Du, R., Chen, W., Xing, X. Q., Mo, G., Chen, Z. J., Cai, Q. & Sun, D. B. (2014). *J. Phys. Chem. C*, **118**, 11454–11463.